Synthetic Methods

DOI: 10.1002/anie.201209535

Template-Free Synthesis of VO_2 Hollow Microspheres with Various Interiors and Their Conversion into V_2O_5 for Lithium-Ion Batteries**

*Anqiang Pan, Hao Bin Wu, Le Yu, and Xiong Wen (David) Lou**

Hollow micro- and nano-structures have attracted great interest because of their promising applications in a wide range of areas.[1–3] Substantial efforts have been dedicated to the facile synthesis of hollow structures with different complex interiors, such as core-shelled,[2] yolk-shelled,[2,4] and multi-shelled hollow structures,[5,6] in view of their fantastic architectures and tunable physical and chemical properties, which are attractive for many applications, such as drug delivery,[4,7,8] photocatalysis,[9–11] dye-sensitized solar cells,[12,13] gas sensors,[14] and lithium-ion batteries (LIBs).[15–17] A common synthetic strategy for the fabrication of hollow structures with complex interiors employs sacrificial templates, such as uniform polymer,[18,19] silica,[5,7] carbon,[14,20] and metal oxide nanoparticles.[5] For example, multi-shelled metal oxide hollow spheres, including TiO_2, iron oxides, and SnO_2, have been synthesized by employing sacrificial templates.[6,14,18] Multi-shelled Cu_2O hollow spheres have also been prepared through vesicle templating and an intermediate-templating phase-transformation process by Xu et al.[21] However, templating methods for constructing complex hollow structures are usually time consuming and costly because of the need for the synthesis of the templates and the multi-step templating process. Therefore, it is highly desirable to develop facile, scalable template-free approaches for the rational synthesis of hollow structures with designed multi-level interior structures.

Vanadium oxides, especially vanadium pentoxide (V_2O_5), have been extensively studied as high capacity cathode materials for LIBs in the past decades.[22–24] In particular, porous or hollow-structured V_2O_5 materials have drawn special interest because of their advantageous features for facile Li^+ ion insertion and good cycling stability.[25–28] However, the controllable fabrication of V_2O_5 hollow structures with high uniformity and complex interiors through simple synthesis procedures still remains very challenging.[29] Herein, we report the controllable synthesis of uniform VO_2 microspheres with various hollow structures, including yolk-shelled, multi-shelled, and single-shelled structures, through a one-step template-free solvothermal method (for detailed experimental procedures, see the Supporting Information). The complex interior structures can be simply tailored by adjusting the solvothermal reaction duration and the concentration of the VOC_2O_4 precursor solution. The resulting VO_2 hollow complex structures are robust and could be readily transformed into V_2O_5 hollow microspheres, which manifest high capacity and good cycling stability when evaluated as cathode materials for LIBs.

The powder X-ray diffraction (XRD) pattern of a representative sample prepared by solvothermal synthesis is shown in Figure 1a. The pattern can be assigned to the recently reported monoclinic VO_2 phase with the lattice parameters of $a = 4.5968$ Å, $b = 5.6844$ Å, $c = 4.9133$ Å, $\beta = 89.39°$.[30] As shown in the low magnification field-emission scanning electron microscope (FESEM) image (Figure 1b), the VO_2 microspheres are highly uniform, with a diameter of around 1 μm. The FESEM image with a higher magnification (Figure 1c) shows that the surface of the microspheres is composed of small nanoplates with a thickness of around 20 nm. The interior structure of the microspheres was investigated by transmission electron microscopy (TEM)

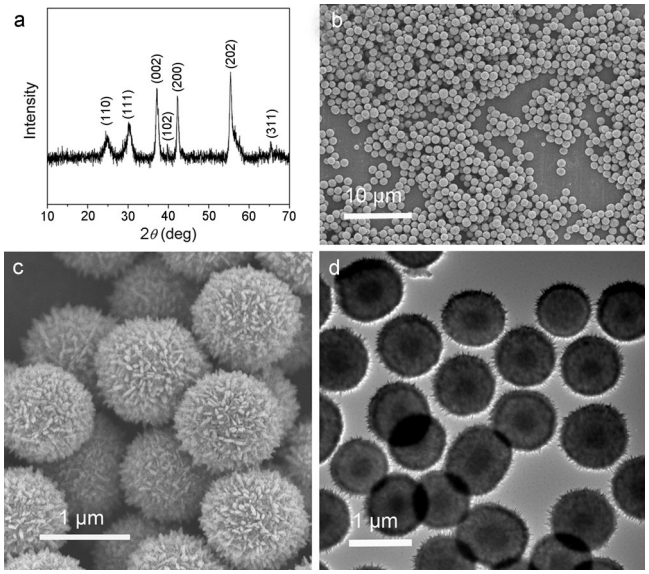

Figure 1. XRD pattern (a), FESEM images (b,c) and TEM image (d) of the VO_2 microspheres prepared at 200 °C after solvothermal reaction for 2.5 h.

[*] Dr. A. Q. Pan,[+] H. B. Wu,[+] L. Yu, Prof. X. W. Lou
School of Chemical & Biomedical Engineering, Nanyang Technological University, 62 Nanyang Drive
637459, Singapore (Singapore)
E-mail: xwlou@ntu.edu.sg
Homepage: http://www.ntu.edu.sg/home/xwlou/
[+] These authors contributed equally to this work.

[**] The authors acknowledge financial support from the Institute of Nanosystems Interface Science and Technology (INSIST) at Nanyang Technological University.

Supporting information for this article, including experimental procedures, additional FESEM and TEM images, nitrogen adsorption-desorption measurement results, and additional electrochemical data, is available on the WWW under http://dx.doi.org/10.1002/anie.201209535.

and the result is shown in Figure 1 d. The VO_2 microspheres possess a yolk-shelled structure, with a shell of about 100 nm thickness and a spherical core of about 400 nm diameter. The large void space between the shell and the interior core can be easily recognized owing to its relatively low contrast in the TEM image. Such highly uniform yolk-shelled VO_2 microspheres have rarely been synthesized before.

Time-dependent experiments were carried out to investigate the formation process of the yolk-shelled structure and the possibility of constructing other complex interior structures. The structures and morphologies of the solvothermally prepared products are characterized by FESEM and TEM. As shown in Figure 2 a and b, the microspheres obtained after

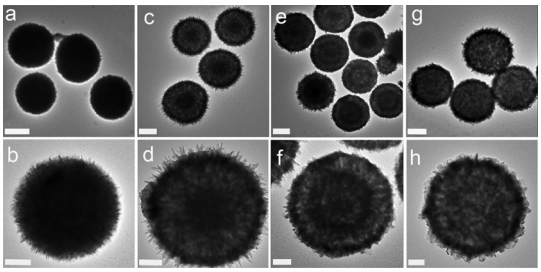

Figure 2. TEM images of the VO_2 microspheres prepared with different reaction durations. a, b) 2 h; c, d) 2.5 h; e, f) 4 h; g, h) 12 h. The scale bars in a, c, e, and g are 0.5 μm, and the scale bars in b, d, f, and h are 200 nm.

solvothermal treatment for only 2 h were found to be completely solid and some small nanoplates are visible on the surface of the microspheres. The FESEM image of a broken microsphere (Supporting Information, Figure S1) further reveals the solid interior structure. Moreover, it can be seen that the solid microspheres are composed of closely packed nanoparticles. Figure 2 c,d shows TEM images of the yolk-shelled VO_2 microspheres obtained after solvothermal treatment for 2.5 h, which are from the same sample shown in Figure 1. A gap distance of about 200 nm is clearly observed between the core and the shell. The transformation from the solid microspheres to the yolk-shelled structures is believed to result from an inside-out Ostwald-ripening process, which commonly refers to the growth of the outer crystalline shell of the solid particles by the consumption and re-crystallization of the interior material.[1,3] However, the Ostwald-ripening process typically results in simple hollow structures with a single shell and a completely void interior.[31–33] In the present system, the dissolution process mainly takes place in the particular region beneath the surface layer, whereas the interior core remains mostly intact. The formation of the interior core could possibly be associated with the relatively large particle size of the microspheres and the poor solubility of vanadium oxide in the solvent. Upon further prolongation of the reaction time, double-shelled or even triple-shelled uniform microspheres can be obtained (Figure 2 e,f). The formation of such multi-shelled structures might be explained by the repeated Ostwald-ripening process taking place on the pre-formed solid cores (the interior core of the yolk-shelled microspheres shown in Figure 2 c,d). The interior architectures, including the solid cores and inner shells, are not thermodynamically stable. After prolonged solvothermal reaction at 200 °C for 12 h, the microspheres eventually evolve into completely hollow spheres with a diameter of about 1300 nm and a shell thickness of about 150 nm (Figure 2 g,h). The possible mechanism to account for the formation of these complex hollow structures, the localized Ostwald-ripening process, is also evidenced by the growth of nanoplates on the surface of the microspheres and the slightly increased diameter upon longer solvothermal reaction, whereas the uniformity of the microspheres is well preserved during the evolution of interior architectures (Figure S2).

Scheme 1 shows the time-dependent interior structural evolution of the VO_2 microspheres. Vanadium oxide nanoparticles are first generated by the hydrolysis of VOC_2O_4 and

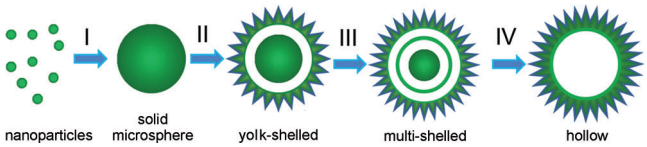

Scheme 1. Time-dependent interior structural evolution of the VO_2 microspheres.

then aggregation to form solid microspheres in stage I. Then the solid spheres undergo the initial inside-out Ostwald-ripening process and transform to the yolk-shelled structure (stage II). With extended solvothermal reaction, secondary Ostwald-ripening takes place on the pre-formed solid cores, resulting in formation of the multi-shelled structure (stage III). Finally, completely hollow microspheres are obtained as a result of the thorough dissolution and re-crystallization of the less stable interior architectures (stage IV). Hence, the interior structure of the VO_2 microspheres could be effectively tailored by simply controlling the reaction duration.

The morphology and size of the products can also be tuned by adjusting the concentration of VOC_2O_4 in the precursor solution. As shown in Figure S3, the concentration of the VOC_2O_4 solution significantly affects the diameter of the uniform VO_2 spheres. Typically, spherical VO_2 aggregates with a uniform size of 250 nm are obtained with a VOC_2O_4 concentration of 0.065 M. When a concentration of 0.082 M is used, VO_2 spheres with a mean diameter of 450 nm are obtained. The average diameters of the VO_2 spheres prepared with concentrations of 0.11 M and 0.165 M are 520 and 700 nm, respectively. Moreover, the surface of the VO_2 spheres becomes rougher with increasing concentration. Similarly, the amount of VOC_2O_4 precursor solution added also has significant effect on the structure and size of the product particles. The size of the uniform spheres increases when more of the VOC_2O_4 precursor solution is added into the reaction solution. More specifically, the VO_2 spheres prepared with 1 mL of VOC_2O_4 solution (0.33 M) exhibit a poorly-defined double-shelled interior structure, whereas the sample prepared with 2 mL of the same solution shows a single-shelled structure with a relatively small void space (Figure S4).

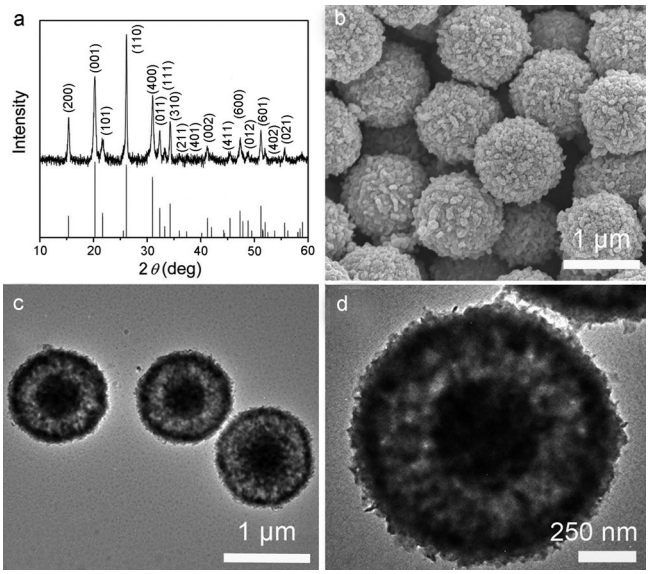

Figure 3. XRD pattern (a), FESEM image (b), and TEM images (c,d) of the yolk-shelled V_2O_5 microspheres obtained by annealing VO_2 in air.

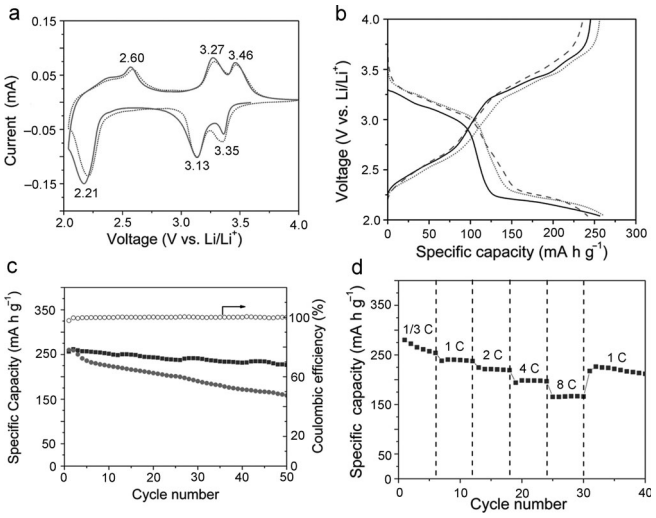

Figure 4. Electrochemical characterization of yolk-shelled V_2O_5 microspheres. a) First two consecutive CV curves; 1st cycle (——), 2nd cycle (•••••). b) Discharge–charge curves of the 1st (——), 2nd (•••••), and 30th (– – –) cycles. c) Specific discharge capacity of yolk-shelled V_2O_5 (■) and solid V_2O_5 (●) microspheres, and the coulombic efficiency (○) of yolk-shelled V_2O_5 versus cycle number at a constant current density of 300 mA g^{-1} in the voltage range of 2–4 V vs. Li/Li^+. d) Rate performance of yolk-shelled V_2O_5 microspheres in the voltage range of 2–4 V vs. Li/Li^+. 1 C = 300 mA g^{-1}.

The VO_2 microspheres can be easily converted into V_2O_5 microspheres by annealing in air at 350 °C for 2 h. The representative XRD pattern shown in Figure 3 a characterizes the phase purity and crystallinity of the obtained V_2O_5 microspheres. All of the diffraction peaks can be unambiguously indexed and assigned to the orthogonal V_2O_5 phase (JCPDS card no. 41-1426, space group: *Pmmn (56)*, $a = 11.516$ Å, $b = 3.566$ Å, $c = 3.777$ Å).[24,28] No other phase is detected, which indicates the high purity of the V_2O_5 microspheres. The morphology and detailed structure of the V_2O_5 microspheres obtained from the yolk-shelled VO_2 microspheres (Figure 1) were further investigated by FESEM and TEM. A view of the product (Figure 3 b) reveals that the V_2O_5 microspheres are highly uniform, with a similar size to the pristine VO_2 microspheres. TEM images (Figure 3 c,d) also reveal that the yolk-shell structure is perfectly preserved after the calcination. There is no discernible shrinkage or structural deformation in the V_2O_5 microspheres, except for the less pronounced nanoplates on the surface, which suggests excellent structural stability. As determined by nitrogen adsorption–desorption measurements (Figure S5), the yolk-shelled hollow spheres give rise to a moderate Brunauer–Emmett–Teller (BET) surface area of 28 $m^2 g^{-1}$ with a pore volume of 0.15 $cm^3 g^{-1}$. The pore size distribution plot indicates the presence of mesopores, which are mainly from the interparticle voids within the shell. Uniform V_2O_5 spheres with different sizes and interior structures can also be easily obtained by annealing the corresponding VO_2 spheres, thus demonstrating the feasibility and versatility of this approach (Figures S6 and S7). Even after annealing at an elevated temperature of 500 °C, the spherical morphology is still well retained, again suggesting excellent structural stability, whereas the surface becomes rougher due to the growth of primary nanocrystallites (Figure S8).

The electrochemical properties of the yolk-shelled V_2O_5 microspheres were first evaluated by cyclic voltammetry. Figure 4 a shows the first two consecutive cyclic voltammograms (CVs) of the electrode prepared from the yolk-shelled V_2O_5 hollow microspheres in the voltage range of 2–4 V vs. Li/Li^+. The three cathodic peaks at the potentials of 3.35, 3.13, and 2.21 V indicate the multi-step lithium ion insertion process in the active materials, and correspond to the phase changes of from α-V_2O_5 to ε-$Li_{0.5}V_2O_5$, then δ-LiV_2O_5, and finally γ-$Li_2V_2O_5$, respectively.[22,23,34] The observed anodic peaks at the potentials of 2.60, 3.27, and 3.46 V correspond to the lithium de-intercalation and the successive backward transformation of the phase from γ-$Li_2V_2O_5$ to δ-LiV_2O_5, ε-$Li_{0.5}V_2O_5$, and α-V_2O_5, respectively.[35] The CV curves are almost identical in the first two cycles, which indicates good reversibility in the electrochemical processes. Figure 4 b shows the discharge and charge curves for the 1st, 2nd, and 30th cycles, which are obtained at a constant current density of 300 mA g^{-1}. Consistent with the above CV results, multiple poorly-defined voltage plateaus related to the lithium ion intercalation and de-intercalation are clearly observed. The first two plateaus, at approximately 3.35 and 3.1 V, are ascribed to the phase transitions from α-V_2O_5 to ε-$Li_{0.5}V_2O_5$, and from ε-$Li_{0.5}V_2O_5$ to δ-LiV_2O_5, respectively. The plateau at approximately 2.2 V is attributed to the formation of the γ-$Li_2V_2O_5$ phase, which results from the intercalation of the second lithium ion into δ-LiV_2O_5.

A high specific discharge capacity of 256 mA h g^{-1} can be obtained in the first cycle within a voltage range of 2–4 V. The value increases slightly to 262 mA h g^{-1} in the second cycle, which realizes over 90 % of the theoretical capacity (290 mA h g^{-1}). As can be seen from Figure 4 b, the voltage profiles are generally retained over repeated discharging and

charging, which again indicates the good electrochemical reversibility and stability of the yolk-shelled V_2O_5 microspheres. Figure 4c shows the discharge capacity and corresponding Coulombic efficiency as a function of cycle number at a constant current density of 300 mA g^{-1}, which corresponds to a rate of about 1 C. After a small initial increase of the discharge capacity in the second cycle, the sample exhibits remarkable capacity retention upon prolonged cycling with a high Coulombic efficiency of nearly 100%. A specific discharge capacity of 227 mA h g^{-1} can be retained in the 50th cycle, which corresponds to 89% of the initial discharge capacity. The cycling performance of solid V_2O_5 microspheres is also given for comparison, which obviously exhibits less satisfactory capacity retention. With a narrower voltage window of 2.5–4 V applied, the yolk-shelled V_2O_5 microspheres can deliver a specific capacity of about 140 mA h g^{-1} with almost no fading over 100 cycles (Figure S9). The hollow and multi-shelled V_2O_5 microspheres also exhibit comparable cycling stability (Figure S10). The electrochemical performance is significantly improved compared to that of the previously reported V_2O_5 nanoparticles[36,37] and even many porous or hollow spheres[15,26,27] with the same voltage window applied. The rate performance of the sample is shown in Figure 4d, and demonstrates facile Li^+ ions insertion/deinsertion in the yolk-shelled nanostructure. The excellent electrochemical performance of such V_2O_5 microspheres might be related to the unique yolk-shell structure of the microspheres in several aspects. First, the nanoscale building blocks in the core and the shell facilitate the transport of lithium ions and electrons. Furthermore, the void space within the microspheres and the porous shell ensure efficient electrolyte penetration and increase the contact area between the electrode and electrolyte. Finally, the microspheres would effectively suppress the aggregation of the primary nanoparticles and their dissolution into the electrolytes.

In summary, a one-pot template-free solvothermal method has been developed for the controllable synthesis of uniform VO_2 microspheres with different complex interiors, including yolk-shelled and multi-shelled structures. The interior structure and size of the uniform VO_2 spheres can be controlled by varying the reaction duration and concentration of the precursor. The VO_2 hollow spheres can be readily transformed into V_2O_5 hollow spheres without structural deformation by calcination in air. The resultant V_2O_5 hollow microspheres exhibit a high initial reversible capacity of 256 mA h g^{-1} at a current density of 300 mA g^{-1}, and good cycling performance over 50 cycles. Such V_2O_5 yolk-shelled microspheres with improved electrochemical performance might be promising as a high-capacity cathode material for future lithium-ion batteries after some further engineering.

Received: November 28, 2012
Published online: January 11, 2013

Keywords: electrochemistry · microspheres · nanostructures · vanadium

[1] X. W. Lou, L. A. Archer, Z. Yang, *Adv. Mater.* **2008**, *20*, 3987–4019.
[2] J. Liu, S. Z. Qiao, J. S. Chen, X. W. Lou, X. Xing, G. Q. Lu, *Chem. Commun.* **2011**, *47*, 12578–12591.
[3] Y. Zhao, L. Jiang, *Adv. Mater.* **2009**, *21*, 3621–3638.
[4] J. Liu, S. Z. Qiao, S. B. Hartono, G. Q. M. Lu, *Angew. Chem.* **2010**, *122*, 5101–5105; *Angew. Chem. Int. Ed.* **2010**, *49*, 4981–4985.
[5] X. W. Lou, C. Yuan, L. A. Archer, *Adv. Mater.* **2007**, *19*, 3328–3332.
[6] X. W. Lou, C. Yuan, L. A. Archer, *Small* **2007**, *3*, 261–265.
[7] J. Liu, S. B. Hartono, Y. G. Jin, Z. Li, G. Q. M. Lu, S. Z. Qiao, *J. Mater. Chem.* **2010**, *20*, 4595–4601.
[8] M. Matsusaki, H. Ajiro, T. Kida, T. Serizawa, M. Akashi, *Adv. Mater.* **2012**, *24*, 454–457.
[9] H. Li, Z. Bian, J. Zhu, D. Zhang, G. Li, Y. Huo, H. Li, Y. Lu, *J. Am. Chem. Soc.* **2007**, *129*, 8406–8407.
[10] Y. Zeng, X. Wang, H. Wang, Y. Dong, Y. Ma, J. Yao, *Chem. Commun.* **2010**, *46*, 4312–4314.
[11] X. Li, X. Liu, Y. Ma, M. Li, J. Zhao, H. Xin, L. Zhang, Y. Yang, C. Li, Q. Yang, *Adv. Mater.* **2012**, *24*, 1424–1428.
[12] X. Wu, G. Q. M. Lu, L. Wang, *Energy Environ. Sci.* **2011**, *4*, 3565–3572.
[13] Z. Dong, X. Lai, J. E. Halpert, N. Yang, L. Yi, J. Zhai, D. Wang, Z. Tang, L. Jiang, *Adv. Mater.* **2012**, *24*, 1046–1049.
[14] X. Lai, J. Li, B. A. Korgel, Z. Dong, Z. Li, F. Su, J. Du, D. Wang, *Angew. Chem.* **2011**, *123*, 2790–2793; *Angew. Chem. Int. Ed.* **2011**, *50*, 2738–2741.
[15] J. Liu, H. Xia, D. Xue, L. Lu, *J. Am. Chem. Soc.* **2009**, *131*, 12086–12087.
[16] P. G. Bruce, B. Scrosati, J.-M. Tarascon, *Angew. Chem.* **2008**, *120*, 2972–2989; *Angew. Chem. Int. Ed.* **2008**, *47*, 2930–2946.
[17] L. Zhou, D. Zhao, X. W. Lou, *Adv. Mater.* **2012**, *24*, 745–748.
[18] M. Yang, J. Ma, C. L. Zhang, Z. Z. Yang, Y. F. Lu, *Angew. Chem.* **2005**, *117*, 6885–6888; *Angew. Chem. Int. Ed.* **2005**, *44*, 6727–6730.
[19] X. Wang, X.-L. Wu, Y.-G. Guo, Y. Zhong, X. Cao, Y. Ma, J. Yao, *Adv. Funct. Mater.* **2010**, *20*, 1680–1686.
[20] J. Guan, F. Mou, Z. Sun, W. Shi, *Chem. Commun.* **2010**, *46*, 6605–6607.
[21] H. Xu, W. Wang, *Angew. Chem.* **2007**, *119*, 1511–1514; *Angew. Chem. Int. Ed.* **2007**, *46*, 1489–1492.
[22] Y.-S. Hu, X. Liu, J.-O. Muller, R. Schlogl, J. Maier, D. S. Su, *Angew. Chem.* **2009**, *121*, 216–220; *Angew. Chem. Int. Ed.* **2009**, *48*, 210–214.
[23] R. J. Cava, A. Santoro, D. W. Murphy, S. M. Zahurak, R. M. Fleming, P. Marsh, R. S. Roth, *J. Solid State Chem.* **1986**, *65*, 63–71.
[24] X.-F. Zhang, K.-X. Wang, X. Wei, J.-S. Chen, *Chem. Mater.* **2011**, *23*, 5290–5292.
[25] X. Rui, J. Zhu, D. Sim, C. Xu, Y. Zeng, H. H. Hng, T. M. Lim, Q. Yan, *Nanoscale* **2011**, *3*, 4752–4758.
[26] S. Wang, Z. Lu, D. Wang, C. Li, C. Chen, Y. Yin, *J. Mater. Chem.* **2011**, *21*, 6365–6369.
[27] J. Liu, Y. Zhou, J. Wang, Y. Pan, D. Xue, *Chem. Commun.* **2011**, *47*, 10380–10382.
[28] A.-M. Cao, J.-S. Hu, H.-P. Liang, L.-J. Wan, *Angew. Chem.* **2005**, *117*, 4465–4469; *Angew. Chem. Int. Ed.* **2005**, *44*, 4391–4395.
[29] A. Q. Pan, T. Zhu, H. B. Wu, X. W. Lou, *Chem. Eur. J.* **2013**, *19*, 494–500.
[30] L. Liu, F. Cao, T. Yao, Y. Xu, M. Zhou, B. Qu, B. Pan, C. Wu, S. Wei, Y. Xie, *New J. Chem.* **2012**, *36*, 619–625.
[31] X. Cao, L. Gu, L. Zhuge, W. Gao, W. Wang, S. Wu, *Adv. Funct. Mater.* **2006**, *16*, 896–902.
[32] J. Yu, H. Guo, S. A. Davis, S. Mann, *Adv. Funct. Mater.* **2006**, *16*, 2035–2041.

[33] Y. Wang, Q. Zhu, H. Zhang, *Chem. Commun.* **2005**, 5231 – 5233.
[34] A. Q. Pan, J. G. Zhang, Z. M. Nie, G. Z. Cao, B. W. Arey, G. S. Li, S. Q. Liang, J. Liu, *J. Mater. Chem.* **2010**, *20*, 9193 – 9199.
[35] A. Odani, V. G. Pol, S. V. Pol, M. Koltypin, A. Gedanken, D. Aurbach, *Adv. Mater.* **2006**, *18*, 1431 – 1436.
[36] S.-H. Ng, T. J. Patey, R. Büchel, F. Krumeich, J.-Z. Wang, H.-K. Liu, S. E. Pratsinis, N. Petr, *Phys. Chem. Chem. Phys.* **2009**, *11*, 3748 – 3755.
[37] Y. L. Cheah, V. Aravindan, S. Madhavi, *J. Electrochem. Soc.* **2012**, *159*, A273 – A280.

